Optimization of a Light Guide in PMT based Large-area Phoswich Detectors for Simultaneous Alpha/beta Detection

Wooseub Kim[a], Jinhwan Kim[a], Giyoon Kim[a], Kyeongjin Park[a], Kilyoung Ko[a], Jisung Hwang[a] and Gyuseong Cho[a*]
[a]*Dept of Nuclear and Quantum Engineering, Korea Advanced Institute of Science and Technology, Daejeon 291*
[*]*Corresponding author: gscho1@kaist.ac.kr*

1. Introduction

About 50 % of Nuclear Power Plants (NPPs), which were constructed based on Generation II reactor, have been operated for more than 30 years in the world. Typically, the reactor has an original design life time of 40 years. In this respect, decommissioning old NPPs is an inevitable task.

According to the Multi-Agency Radiation Survey and Site Investigation Manual (MARSSIM), measuring the average contamination level and distribution of alpha, beta and gamma rays at contaminated areas such as soil and building is required for area classification as an initial step of decommissioning [1]. For the pre-survey, Phoswich (Phosphor sandwich) detector has an advantage that simultaneous detection of alpha and beta rays is available with large cross sectional area, which can be easily manufactured.

Detection efficiency of a large-area phoswich detector is directly influenced by light collection efficiency, which is an indicator that how many visible lights are conserved and delivered from scintillator to Photomultiplier tube (PMT). By coupling an optimal light guide between scintillator and PMT, it is possible to enhance light collection efficiency, and consequently reduce Minimum Detectable Concentration (MDC) in relation to the residual radioactivity criteria [1].

In this research, to identify the optimal thickness of a light guide in PMT based large-area phoswich detectors for simultaneous detection of alpha and beta rays, commercially-available optical design software lighttools was used for the simulation of light transport and experiments were conducted to verify the simulation result. As a result, the optimal thickness was figured out depending on the coupled scintillator area of 100×100 mm^2, 150×150 mm^2 and 200×200 mm^2.

2. Materials and methods

2.1. Description of the phoswich detector

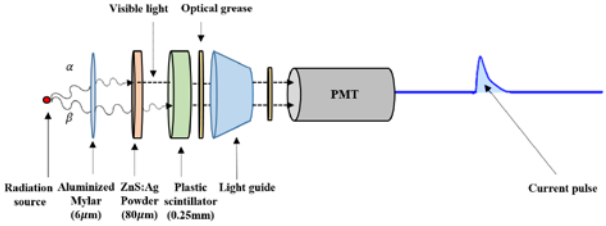

Fig. 1. Schematic of ZnS:Ag/Plastic phoswich detector.

Basically, the designed phoswich detector are composed of 6 μm thick aluminized mylar, 80 μm thick ZnS:Ag powder (Eljen, EJ-600), 0.25 mm thick plastic scintillator (Eljen, EJ-212), 0.1 mm thick optical grease (Saint-Gobain, BC-630), light guide and PMT (Hamamatsu photonics, R6233) of 3-inch (76.2 mm) photocathode diameter (Fig. 1).

To minimize the loss of generated visible lights from a scintillator, teflon (PTFE) is covered on the side of a light guide. Likewise, to remove an air layer and smoothly connect scintillator, light guide and PMT, optical grease is used.

2.2. Simulation of light transport

As radiation particles deposit their energy in a scintillator, this energy is partially converted into visible lights. In the case of ZnS:Ag powder, wavelength of maximum emission is 450 nm. For plastic scintillator, wavelength of maximum emission is 423 nm [2]. Furthermore, the PMT only responds to visible lights in a limited wavelength range from 300 nm to 650 nm, and the most sensitive wavelength region is 420 nm [3]. Therefore, the most concerned wavelength range is from 420 nm to 450 nm for the simulation of light transport. Components of the phoswich detector, which affect the motion of visible lights generated from a scintillator, are summarized with optical properties in table I [2, 4-10].

ZnS:Ag scintillator has 300 light output (% Anthracene) which is relatively higher than plastic scintillator with 65 light output (% Anthracene) [2]. Moreover, the thickness of ZnS:Ag powder is much thinner than plastic scintillator (Fig. 1). In other words, the plastic scintillator occupies most of the scintillating region, and the number of generated visible lights at plastic scintillator is smaller than that of ZnS:Ag powder. Loss of generated visible lights at plastic scintillator can be directly linked to weak signals of PMT rather than ZnS:Ag powder. Thus, only plastic scintillator was considered for the simulation.

Table I: Optical properties of components in the phoswich detector at 420-450 nm wavelength.

Optical properties (Unit)	Type (Composition)	Value
Refractive index (None):	Light guide (PMMA)	1.502
	Optical grease (Silicone)	1.465
	Plastic scintillator (Polyvinyltoluene)	1.58

Attenuation length (cm):	Plastic scintillator (Polyvinyltoluene)	250
Transmission (%):	Light guide (PMMA)	92
	Optical grease (Silicone)	98
Reflectivity (%):	Aluminized mylar (Aluminum)	92.6
	Teflon (PTFE)	98

In terms of simulation conditions, unpolarized mode was used because the generated visible lights from a scintillator has no specific polarization. Snell's law was also used to indicate the angle of the refracted visible light by assuming ideally polished surfaces. On the bottom of the scintillator, reflection taking place at the aluminized mylar was considered. However, lambertian scattering, which defines diffusely reflecting surface, was applied to the side of a light guide because of the taped teflon (Fig. 2). The distribution of scattered intensity is given by the following equation (1) [11].

$$P(\theta) = P_0 \cos(\theta), \quad (1)$$

where $P(\theta)$ is the intensity or radiance independent of the incident angle which varies only as a function of the cosine of the scattered angle, and P_0 is the intensity or radiance in the normal direction.

In scanning contaminated areas, the residual radioactive sources are unknown. Therefore, it is assumed that the sources are uniformly distributed, and evenly involve interactions with the detector. In this principle, 10,000,000 visible lights were generated randomly but uniformly at the volume of plastic scintillator. All visible lights, which passed through the light collection surface, were counted with less than 5 % of relative error. The simulated geometry is shown in Fig. 3. and Table II.

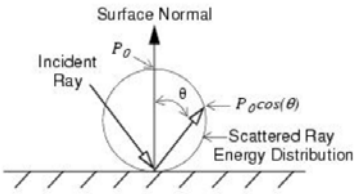

Fig. 2. The Lambertian scatterer in 'Lighttools'.

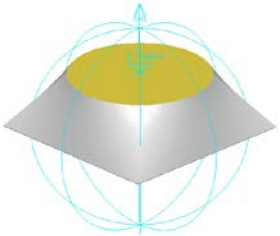

Fig. 3. The simulated geometry for light transport.

Table II: Description of the simulated geometry.

Geometry	Type	Value (mm)
	Diameter of light collection surface (D1)	76.2 (Fixed)
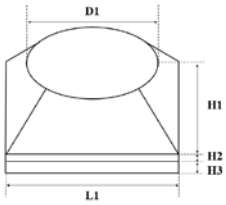	Thickness of light guide (H1)	0, 10, 20, 30, 40, 50, 80, 100
	Thickness of optical grease (H2)	0.1 (Fixed)
	Thickness of plastic scintillator (H3)	0.25 (Fixed)
	Length of plastic scintillator (L1)	100, 150, 200

2.3. Experimental measurements

For experimental measurements, 100×100 mm^2 areal ZnS:Ag/plastic scintillator and light guides of 10 mm, 20 mm, 30 mm and 50 mm thickness (Fig. 4) were coupled to the phoswich detector, which is illustrated in Fig. 1. Radioactive sources of 50 mm diameter such as C-14, Tc-99 and 40 mm diameter like Cl-36 (Fig. 5) were positioned 10 mm away from the scintillator of the detector. Besides, these were located under the center and also corner of the scintillator to verify the optimal thickness of a light guide because radioactive sources have smaller area than the scintillator (Fig. 6).

To count interactions induced by beta rays from a radioactive source, the detector was connected to a digitizer (Caen, DT5725) which digitizes PMT anode pulses and performs the analysis. To minimize the effect of extraneous light, experiments were conducted inside of a dark box under the background radiation level of 10μR/hr (Fig. 7). Background count rates were measured less than 300cpm in any case.

Fig. 4. Light guides of 10 mm, 20 mm, 30 mm and 50 mm thickness.

Fig. 5. Radioactive sources for the experiments.

Fig. 6. Radioactive source position under the center (1) and corner (2) of the scintillator.

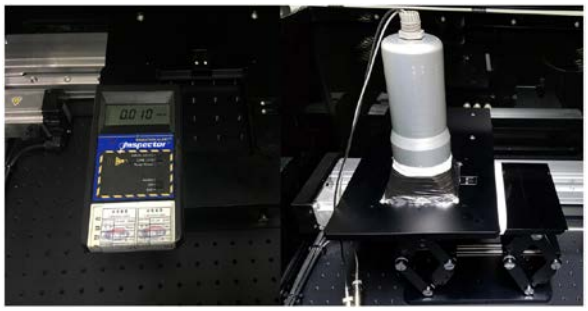

Fig. 7. Background count rate at the experimental environment.

Instrument efficiency (e_i), which is affected by light collection efficiency, was derived by the following equation (2) [12].

$$e_i = \frac{R_{S+B} - R_B}{q_{2\pi}}, \quad (2)$$

where R_{S+B} is the gross count rate of the measurement in cpm, R_B is the background count rate in cpm, and $q_{2\pi}$ is the 2π surface emission rate in cpm. For the uncertainty of an instrument efficiency (σ_i) was calculated by the following equation (3).

$$\sigma_i = \frac{\sqrt{\sigma_{S+B}^2 + \sigma_B^2}}{q_{2\pi}}, \quad (3)$$

where σ_{S+B} is the uncertainty of gross count rate in cpm, and σ_B is the uncertainty of background count rate in cpm.

To minimize the fluctuation of background count rate, background count rates were measured five times for 3,600 seconds, and gross count rates were measured five times for 180 seconds.

3. Results and discussion

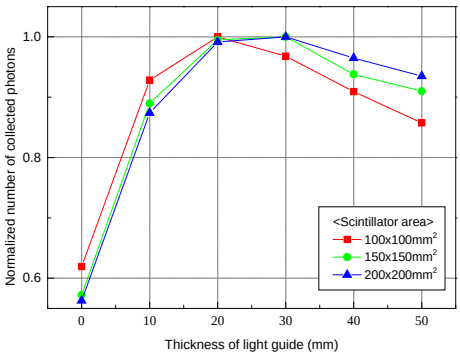

Fig. 8. The simulation result of collected visible lights in relation to thickness of the light guide (H1) and length of the scintillator (L1).

The light transport simulation showed that light collection was the highest when the thickness of a light guide is 20 mm for 100×100 mm^2 areal scintillator, 30 mm for 150×150 mm^2 areal scintillator, and 30 mm for 200×200 mm^2 areal scintillator (Fig. 8).

In experiments, instrument efficiency was the highest with 20 mm thick light guide when radioactive sources were positioned under the center or corner of 100×100 mm^2 areal scintillator (Fig. 9). However, unlike simulation results, instrument efficiency with 10 mm thick light guide tends to be higher than the efficiency with 30 mm thick light guide. It seems that this result came out from unlikeness induced by the process of covering teflon manually and manufacturing light guides.

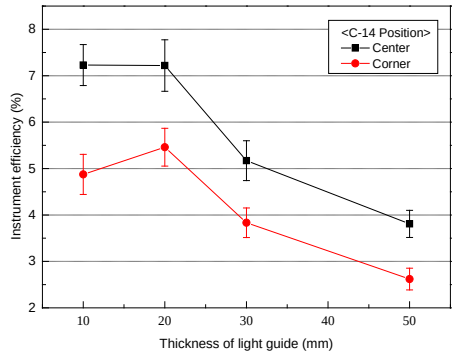

(A)

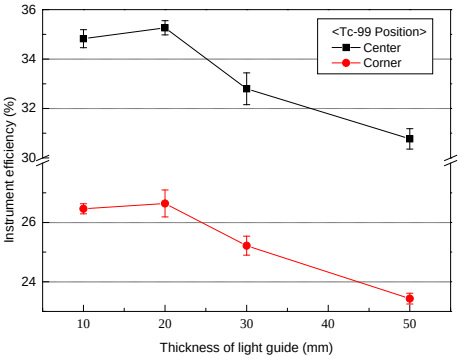

(B)

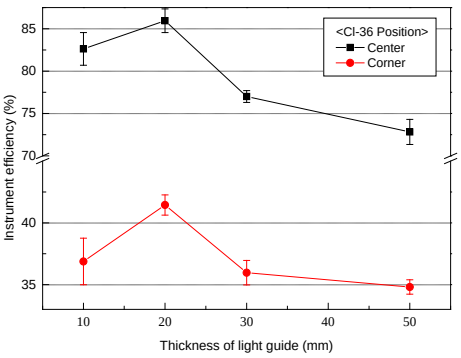

(C)

Fig. 9. Variation of instrument efficiency depending on the thickness of light guide with (A) C-14, (B) Tc-99 and (C) Cl-36 radioactive sources.

4. Conclusion

In this research, when the thickness of light guide initially increased, generated visible lights tended to move well to the light collection surface because lambertian reflectance occurs at the side of a light guide. However, after a certain thickness, the number of collected lights decreased. As the thickness of light guide increases, visible lights should pass through a longer distance inside the light guide with more possibilities to be absorbed. Therefore, both of effects should be considered to define the optimal thickness of a light guide.

In addition to that, when radioactive sources were located under the center of the scintillator rather than the corner, instrument efficiency was relatively high. It shows that centrally located radioactive sources can cause more interactions geometrically with a large solid angle, and visible lights generated from the center of a scintillator can easily reach a PMT window.

When radioactive sources are smaller than the scintillator of the phoswich detector, instrument efficiency is overestimated due to a large solid angle between the source and the detector. For this reason, as a further research, large-area radioactive sources will be used for optimization of large-area phoswich detectors for simultaneous alpha/beta detection.

5. Acknowledgements

This work was supported by the Center for Integrated Smart Sensors funded by the Ministry of Science and ICT as Global Frontier Project (CISS-2016M3A6A6929965).

REFERENCES

[1] U.S. Nuclear Regulatory Commission, Multi-Agency Radiation Survey and Site Investigation Manual (MARSSIM), NRC; NUREG-1575, Rev. 1, 2000.
[2] Eljen Technology, Alpha/Beta Detection EJ-444, 2016. http://www.eljentechnology.com/products/zinc-sulfide-coated/ej-444.
[3] Hamamatsu Photonics, Photomultiplier Tubes Opening The future with Photonics, 2005. http://sales.hamamatsu.com/assets/pdf/catsandguides/PMT_TPMO0005E03.pdf.
[4] Eljen Technology, Light Guides and Acrylic Plastic, 2016. http://www.eljentechnology.com/products/light-guides-and-acrylic-plastic.
[5] Szczurowski, Refractive index and related constants-Poly(methyl methacrylate) (PMMA, Acrylic glass), 2014. https://refractiveindex.info/?shelf=organic&book=poly(methyl_methacrylate)&page=Szczurowski.
[6] G. Hass, J.E. Waylonis, Optical Constants and Reflectance and Transmittance of Evaporated Aluminum in the Visible and Ultraviolet, Journal of the Optical Society of America, Vol.51, p.719,1961.
[7] T.Gogami, N.Amano, S.Kanatsuki, T.Nagae, K.Takenaka, Development of Water Cerenkov Detector for On-line Proton Rejection in Hypernuclear Spectroscopy via the (K^-, K^+) Reaction, Nuclear Instruments and Methods in Physics Research A, Vol.817, pp.70-84, 2016.
[8] Saint-Gobain Crystals, Detector Assembly Materials, 2016. https://www.crystals.saint-gobain.com/sites/imdf.crystals.com/files/documents/detector-assembly-materials_69673.pdf.
[9] Berghof, Optical PTFE The reference for light. https://www.berghof-fluoroplastics.com/fileadmin/Dateien-Einpflege/Seitenbaum/Home-Downloads/Produkte/PTFE-Produkte/Optisches%20PTFE/Berghof_PTFE-Products_Optical-PTFE.pdf.
[10] Eljen Technology, General Purpose Plastic Scintillator EJ-200, EJ-204, EJ-208, EJ-212, 2016. https://www.berghof-fluoroplastics.com/fileadmin/Dateien-Einpflege/Seitenbaum/Home-Downloads/Produkte/PTFE-Produkte/Optisches%20PTFE/Berghof_PTFE-Products_Optical-PTFE.pdf.
[11] Synopsys Inc, LightTools. https://www.synopsys.com/optical-solutions/lighttools.html.
[12] U.S. Nuclear Regulatory Commission, Minimum Detectable Concentrations with Typical Radiation Survey Instruments for Various Contaminants and Field Conditions, NRC; NUREG-1507, 1998.